# Origin of Heterogeneous Relaxation in a Random Liquid Crystal Thermoset Copolyester

**Gordon J. Kearley,*,† Theo J. Dingemans,‡ Olga Kruglova,† John Stride,§ and Fokko M. Mulder†**

*Interfaculty Reactor Institute, Delft University of Technology, Mekelweg 15, 2629 JB Delft, The Netherlands; Faculty of Aerospace Engineering, Delft University of Technology, Kluyverweg 1, 2629 HS Delft, The Netherlands; and Institute Laue Langevin, BP156 Grenoble, 38042 Cedex 09, France*

*Received June 30, 2004; Revised Manuscript Received October 12, 2004*

ABSTRACT: The 73/27 random copolyester based on 4-hydroxybenzoic acid (HBA) and 6-hydroxy-2-naphthoic acid (HNA) shows a fast, dispersed relaxation process on the picosecond time scale. The underlying motion is difficult to determine unambiguously, but the data are consistent with translation of chain segments in a direction that is perpendicular to the chain direction. As the temperature is increased from the beta transition (303 K) to the glass transition, $T_g$ (381 K), the dispersion stays constant and the average relaxation time increases slightly. At $T_g$ the dispersion increases abruptly to a new constant value, and the average relaxation time increases noticeably with temperature up to the nematic melt transition, $T_m$ (553 K). This unusual behavior is probably connected to the appearance of a slow relaxation process that becomes discernible above $T_g$. The characteristic length of this slow process remains constant between $T_g$ and $T_m$ at a value that corresponds to the interchain spacing close to $T_m$. This observation is consistent with a crankshaft motion of neighboring aromatic groups. As the amplitude of this motion increases, the average barrier to translation perpendicular to the chain direction becomes higher, causing longer relaxation times for the fast process. The slow crankshaft rotation thus appears to cause the dispersion of the fast translational process.

## Introduction

The liquid-crystalline thermoset copolyester HBA/HNA ("Vectra") consists of 4-hydroxybenzoic acid (HBA) and 6-hydroxy-2-naphthoic acid (HNA) subunits that are randomly organized along the polymer chain with the overall composition being 73:27, respectively. A schematic illustration of HBA/HNA is given in Figure 1. At room temperature until its glass transition at 383 K the polymer chains are aligned, and there is some approximate registry between the composition and local structure of segments in neighboring segments.[11] The aligned character is preserved above $T_g$ and across the transition into a nematic melt at 553 K.[3]

The different phases are characterized by increasingly different dynamics. In the present paper we will show that the dynamics of this material on the picosecond time scale is particularly interesting because we can discern two types of local dynamics: a fast process (∼1 ps) that is dispersed and a slow process (∼60 ps) that will cause the dispersion in the fast process. This arises from the difference in time scales of around 2 orders of magnitude so that there is no coupling between the two processes; the slow process simply provides a distribution of environments in which the fast process occurs. The main challenge in the present study is to elucidate the nature of the fast and slow processes and their relation to the phase behavior. Both types of motion are easily measured in a single experiment using quasi-elastic neutron scattering (QENS), and we will show that by studying the variation of peak widths and intensities as a function of momentum transfer and temperature it is possible to achieve a consistent picture of the fast and slow dynamics and how the latter causes dispersion.

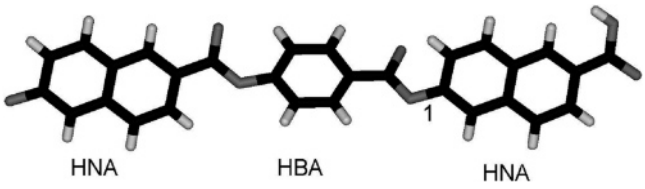


**Figure 1.** Illustration of copolyester HBA/HNA: 4-hydroxybenzoic acid (HBA) and 6-hydroxy-2-naphthoic acid (HNA). HBA and HNA are arranged randomly in the chain with an overall ratio of 70:30, respectively.

Dispersed dynamics of this compound has been reported before on the nanosecond time scale in studies using time-resolved fluorescence emission measurements[1,2] over the 300−500 K range. However, this approach is more related to detailed variations in the electronic structure of the conjugated segments, which is difficult to relate to molecular dynamics directly. There has also been a previous QENS study that first revealed the broader signal (∼1 ps) but due to instrumental limitations was unable to study the profile of this peak accurately or resolve the slower (∼60 ps) component, both aspects being essential to the conclusions presented here. Elastic neutron scattering[4,5] shows the presence of a non-Gaussian parameter in the Debye−Waller factor that suggests a dynamical heterogeneity that exists within a time domain longer than about 1 ps.

The main aim of the present work is to establish an interpretation that is consistent with the two measured

† Interfaculty Reactor Institute, Delft University of Technology.
‡ Faculty of Aerospace Engineering, Delft University of Technology.
§ Institute Laue Langevin.
* Corresponding author. E-mail Kearley@iri.tudelft.nl.

10.1021/ma0486849 CCC: $27.50 
Published on Web 11/25/2004

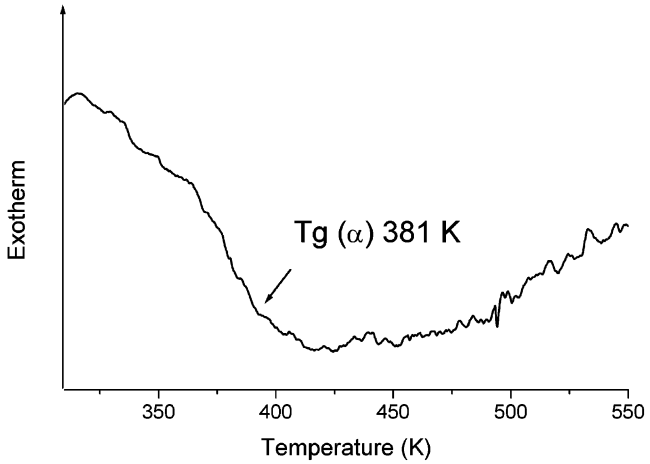


**Figure 2.** DSC (Perkin-Elmer sapphire) trace of cross-linked Vectra over the temperature range of the QENS experiments. A heating rate of 10 K/min was used.

QENS components reported here and with the data presented in the previous studies. The generally accepted phase transitions for non-cross-linked Vectra are[2] $\gamma$(213 K), $\beta$(298 K), $T_g$, or $\alpha$(373 K) and melting at 553 K. Our own DSC measurements for the cross-linked polymer (Figure 2) show a $T_g$ at around 381 K, suggesting that the dynamics associated with this transitions is little changed by cross-linking. We would anticipate that at least one component of the dynamics on the picosecond time scale would be rotation or libration about the skeletal single bonds.[6] Indeed, a molecular dynamics study[7] reveals that the barriers to rotation about the single bond labeled 1 in Figure 1 is 12.5 kJ mol$^{-1}$. Further, ab initio calculations for the gas phase[8] show an angular displacement of adjacent aromatic units of around 60° due to interaction between the carbonyl oxygen and the aromatic-ring hydrogen, the barrier for this torsion being 8.4 kJ mol$^{-1}$. These figures are broadly comparable with the measured activation energy, 8.0 kJ mol$^{-1}$, from QENS[3] of the relaxation process above the melting point (558 K) where the temperature dependence of the peak width becomes Arrhenius. This signal was attributed to free rotation of the aromatic groups. However, below the melting point the intensity of the QENS peak is too weak for this assignment, and also the length scale is too short. Therefore, below the melting point another type of motion is required in order to explain the QENS.

## Materials and Methods

The HBA/HNA liquid crystal thermoset was prepared by cross-linking a 9000 g/mol HBA/HNA oligomer, end-capped with phenylethynyl functionalities. The structure shown in Scheme 1 was synthesized using conventional melt-condensation methods, and the synthetic details are reported elsewhere.[9]

The oligomer was successively processed into thin (0.015 mm), quasi-isotropic films and cross-linked at 648 °C for 1 h. The obtained nematic thermoset film were analyzed using differential scanning calorimetry (DSC), and at various heating and cooling rates we could only detect a $T_g$ at 381 K. Other transitions, such as $T_m$, could not be observed.

Quasi-elastic neutron spectra were obtained using the IN6 spectrometer at the Institut Laue Langevin in Grenoble, France. An incident wavelength of 5.9 Å was selected to give the correct compromise between energy range and energy resolution. The sample was sealed in thin-walled aluminum containers and temperature control was achieved using a standard oven. The sample thickness was chosen to give a scattering probability of 10%. Corrections for detector efficiency, container scattering, sample shape, etc., and conversion of the data to $S(Q,\omega)$ were made using standard algorithms. No attempt was made to orient the samples with respect to the momentum-transfer vector.

## Scattering Law

The variation of quasi-elastic intensity and width with momentum transfer, $Q$, provides information on the spatial distribution of the motion and the characteristic time, respectively. To obtain an initial idea of the number of components in the QENS data and their $Q$ dependence, it is easiest to begin by fitting simple analytical functions. Exponential decay leads to a Lorentzian-shaped quasi-elastic broadening of the neutron spectrum, and below $T_g$, a single Lorentzian function was found to provide a reasonable first approximation to the quasi-elastic spectral component. To separate the quasi-elastic scattering from the elastic scattering, the observed spectra were fitted with the sum of the elastic component (as a single spectral channel) plus a Lorentzian quasi-elastic component, the whole being convoluted with the measured resolution function. The fitted elastic component convoluted with the measured resolution function was then subtracted from the measured spectrum, leaving the purely quasi-elastic component with almost no assumption about its actual functional form. It is important to notice that when these quasi-elastic components from different scattering angles are scaled by $Q$, they all fall on a single curve, as shown in Figure 3. Note that spectra measured at a certain detector are not at constant $Q$ because $Q$ also varies with energy transfer, $\hbar\omega$, according to

$$Q = k_i \sqrt{2 - \frac{\hbar\omega}{E_0} - 2\sqrt{1 - \frac{\hbar\omega}{E_0}}\cos(\theta)} \qquad (1)$$

where $k_i$ is the incident wave vector and $\theta$ is the scattering angle. The actual $Q$ range covered in Figure 3 is from 0.4 to 3.0 Å$^{-1}$. We now need to find the best functional form of the master curve in Figure 3. The broken line shows the best fit using a Lorentzian function that provides only modest agreement. A better fit is achieved by Fourier transforming the data to the

**Scheme 1**

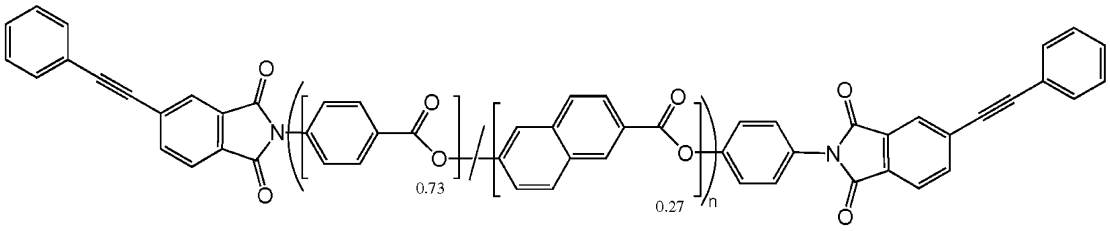

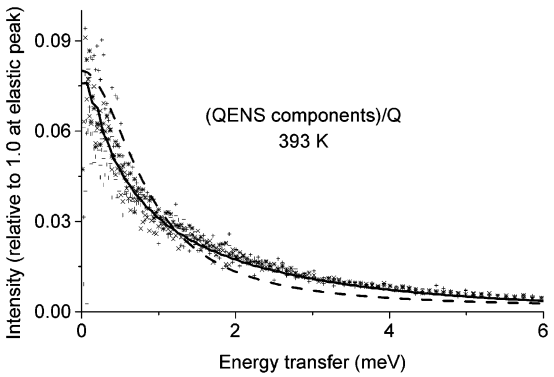


**Figure 3.** QENS data from five scattering angles after removal of the elastic peak. Individual $Q$ values range from 0.36 to 3.0 Å$^{-1}$, depending on both the energy transfer and scattering angle (eq 1), but dividing each observed intensity by its $Q$ value causes the data to fall on a common curve. The solid line is the result of a fit of the Fourier transformed data to a stretched exponential function, with the result back-transformed to the frequency domain. The broken line is the best fit with a Lorentzian function.

time domain and fitting with a stretched exponential function:

$$P(t) = \exp(-(t/\tau)^{\beta}) \tag{2}$$

Here, $P$ is the overall probability that the system is in the initial state, and $\tau$ is the effective relaxation time from the superposition of decay processes. $\beta$ is a stretching parameter that decreases as the distribution of relaxation process increases. The physical significance of $\beta$ depends on the model chosen for the origin of the distribution and is still a point of considerable discussion. The fit illustrated by the solid line in Figure 3 was achieved by Fourier transforming the data to the time domain so that they could be fitted using eq 2 and then transforming the numerical fitted function back into the frequency domain.

There is no analytical Fourier transform of eq 2, and we may either transform our data to the time domain accepting the truncation errors of limited data range or use an approximate function in the frequency domain. Given that eq 2 is phenomenological, we prefer the latter approach and use the function proposed by Bergman:[10]

$$X''(\omega) = \frac{X''_p}{1 - b + \frac{b}{1+b}\left[b\left(\frac{\omega_p}{\omega}\right) + \left(\frac{\omega}{\omega_p}\right)^b\right]} \tag{3}$$

where $X_p$ is the maximum in the susceptibility, $\omega_p$ is the position of the maximum in the susceptibility, and $b$ is a parameter that can be compared with the exponent, $\beta$, in eq 2. The measured frequency spectrum is related to eq 3 divided by $\omega$, which we will indicate by a Bergman spectral contribution to the spectra. When fitting the spectra with Bergman functions above $T_g$, it is clear that a second contribution was required: a narrower Lorentzian function whose behavior is more normal, the width being almost constant with $Q$ and increasing with increasing temperature. The original broader Bergman function continued to become narrower with increasing temperature above $T_g$ and continued to have a non-Lorentzian profile. The additional Lorentzian peak is clearly present, but it is very narrow and weak, particularly at lower temperatures. This makes it essentially impossible to separate this peak from the resolution function at lower temperatures and low $Q$, and in order to circumvent this problem, we constructed a constrained global fitting procedure to fit data as a function of all $Q$ and $\omega$ simultaneously. In summary, the complete function for our data is

$$S(Q,\omega) = \left\{\left[\frac{Q(\omega)}{\omega}\frac{X''_p}{1 - b + \frac{b}{1+b}\left[b\left(\frac{\omega_p}{\omega}\right) + \left(\frac{\omega}{\omega_p}\right)^b\right]}\right] + \left[\frac{\left(\frac{P_1(Q)}{\pi P_2}\right)}{1 + \left(\frac{\omega}{P_2}\right)^2}\right] + \delta_{ep}(Q)\right\} \otimes rf \tag{4}$$

The first part of this function contains only three adjustable parameters: $\omega_p$, $b$, and $X_p$, which are thus all independent of $Q$. The Lorentzian function is described by $P_1$, the intensity that is $Q$-dependent, and $P_2$, the half-width that is constant with $Q$. $\delta_{ep}$ is the intensity of a delta function that is represented by a single spectral point at the elastic peak position, the whole being convoluted with *rf*, the measured resolution function. Fourteen experimental spectra from different scattering angles were fitted simultaneously with the global adjustable parameters: $\omega_p$, $\beta$, $X''_p$, and $P_2$. For spectra taken below $T_g$ the intensity of the Lorentzian function was constrained to zero. In eq 4 the Bergman function has been scaled by $Q$, reflecting the observation (Figure 3) that the experimental quasi-elastic components could be brought to a common curve with this scaling.

It should be noted that $b$ in eq 3 and $\beta$ in eq 2 are comparable, but not identical. Although the fitting parameter in eq 4 is $b$, in our discussion we use $\beta$, which is obtained by transforming the fitted Bergman function to the time domain and fitting with eq 2. This allows our values of $\beta$ to be compared directly with other work that uses stretched exponential descriptions.

## Results and Discussion

Preliminary fitting using "free" Lorentzian functions revealed that the overall width of the quasi-elastic scattering reduces with increasing temperature. This surprising observation is also evident in the raw data (after instrumental correction) as illustrated in Figure 4. Consequently, we analyzed the data more carefully using the global fitting function given in eq 4 that enabled us to fit spectra collected at 14 different scattering angles between 20° and 120° in a single constrained fit. Adequate spectral agreement was achieved without the necessity to include additional background, and attempts to introduce a Debye−Waller factors revealed that the data could be equally well fitted with any value between 0 and 0.04 Å$^2$. We constrained the background and Debye−Waller factor to zero. An example of the spectral agreement for a single spectrum within the global fitting is illustrated in Figure 5 over the energy range of the useful data. The intensity of the elastic peaks and the narrow Lorentzian functions have independent values for each spectrum, but the width of the Lorentzian and the Bergman function, as well as the value of $\beta$, were constrained to a single value for all 14 scattering angles. Equation 4 describes the data well, and we will try to understand the origin of the two spectral features.

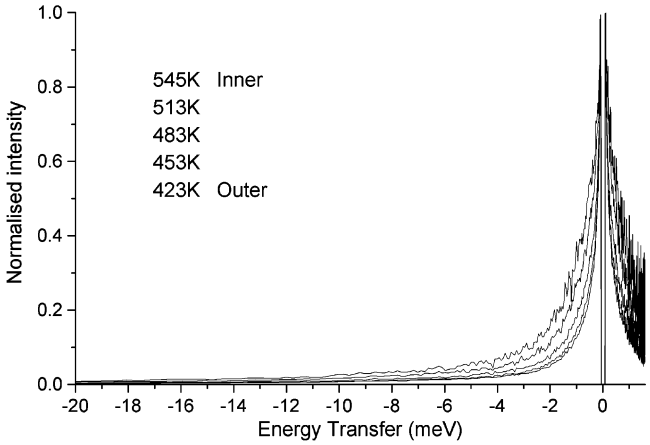


**Figure 4.** Quasi-elastic component at $Q = 1.1$ Å$^{-1}$ in raw data that has only been corrected for detector efficiency and scattering of the sample container. The spectrum at 293 K was subtracted, and the maxima of remaining quasi-elastic components were normalized to unity.

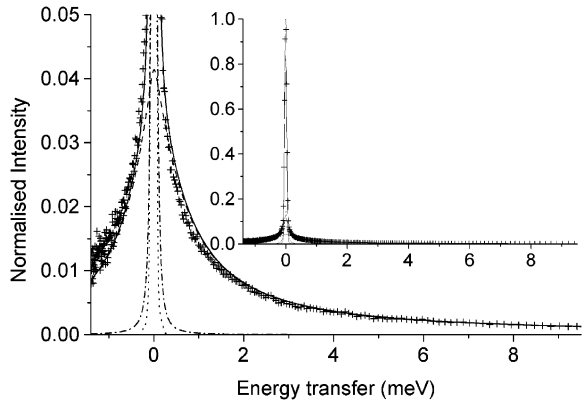


**Figure 5.** An example of the fit per spectrum from the global fitting procedure using eq 4: resolution function (dotted line), slow process (dot−dash line), fast process (dashed line), complete function (solid line). The data (+) are for spectrum 12 (elastic $Q = 1.52$ Å$^{-1}$) out of 14 spectra that were included in the global fit. The plot is a 20× zoom; the unzoomed plot is shown in the inset.

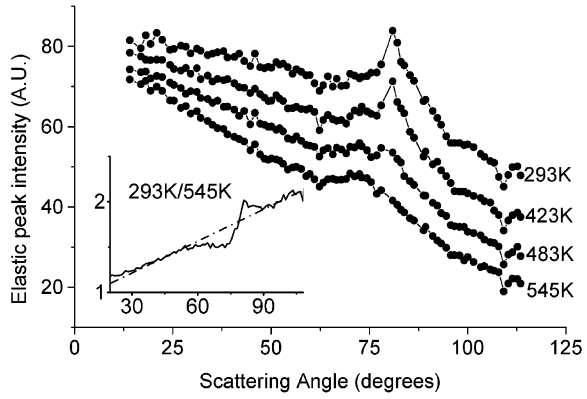


**Figure 6.** Variation of elastic intensity ($\Delta E < 0.02$ meV) as a function of detector angle ($2\theta$). The inset shows the curve for 293 K divided by that for 545 K and reveals the temperature dependence of the diffuse component between ∼60 and 100 $2\theta$ (the straight line is to clarify the difference).

Before discussing the quasi-elastic scattering, there is useful information in the purely elastic scattering, $S(Q)$ at $\omega = 0$, illustrated in Figure 6. These data are the integrated intensity of the three central points in the elastic peak for each detector angle and are a good approximation to purely elastic scattering ($\Delta E < 0.02$ meV). The general loss of intensity with increasing scattering angle and increasing temperature is due to the Debye−Waller factor (which here includes the quasi-elastic scattering), and any deviation from this is due to coherent scattering from structural correlation. The sharp peak at 81° ($2\theta$) in the low-temperature spectra is essentially a Bragg peak that arises from the interchain separation. This peak weakens, broadens, and shifts to smaller angles with increasing temperature, reflecting the lattice expansion perpendicular to the chain direction and an increase in disorder. At all temperatures there is also a broad diffuse elastic signal between about 60° and 100° that is due to a distribution of structural correlations, and because this is essentially elastic scattering ($\Delta E < 0.02$ meV), these must be on a time scale slower than ∼100 ps. Static correlations would show little or no temperature dependence, but by dividing the data at 293 K by those at 545 K (or any other pair), we can see that the diffuse peak (between 60° and 100°) increases in intensity with temperature (see inset in Figure 5: the area below the line is about twice as large as above the line). From the elastic scattering we can conclude that there is a strong dynamical modulation of the interchain distance at all temperatures measured in the present work and that the average interchain correlations increase with temperature.

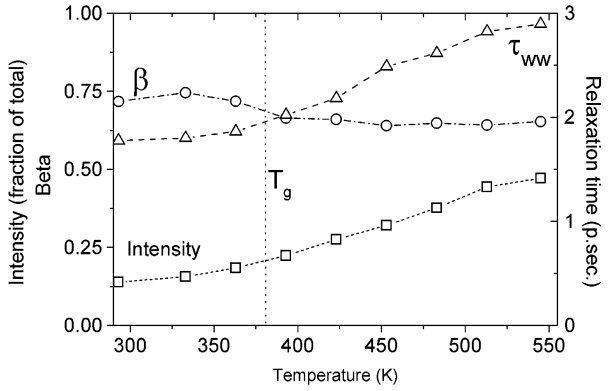


**Figure 7.** Temperature dependence of the fast relaxation process showing the changes at $T_g$, in particular the longer relaxation time with increasing temperature. This process shows dispersed dynamics. The Williams−Watts relaxation time, $\tau_{ww}$, was obtained by mapping eq 3 onto eq 2.

**Phase from 298 to 383 K.** The evolution of the intensity, width, and $\beta$ of the quasi-elastic function with temperature is illustrated in Figure 7. Below $T_g$, a single function is adequate to describe the measured data and reveals that both $\beta$ and the intensity are only weakly temperature dependent in this phase. Interestingly, even in this phase there is a slight, but significant, increase in the average relaxation time as the temperature is increased that we will comment on later.

Koizumi[3] fitted a single Lorentzian function to the quasi-elastic scattering above $T_g$, which clearly corresponds to the broad component that we fit with a Bergman function in the present work. Koizumi found this peak to be polarized normal to the molecular axis, and from the $Q$ dependence of the quasi-elastic width above $T_m$ he found that the underlying motion is compatible with the interchain distance. This strongly suggests the a rotation of the aromatic units. Below $T_m$, and particularly below $T_g$, the quasi-elastic peak-width is almost constant, which is more consistent with a jump

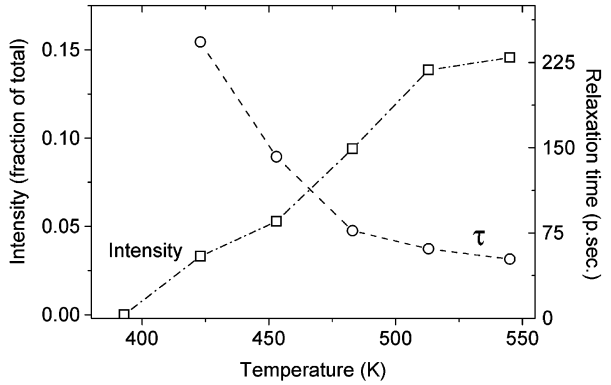


**Figure 8.** Temperature dependence of the slow relaxation process that is only detectable above $T_g$. This process shows a single-exponential decay.

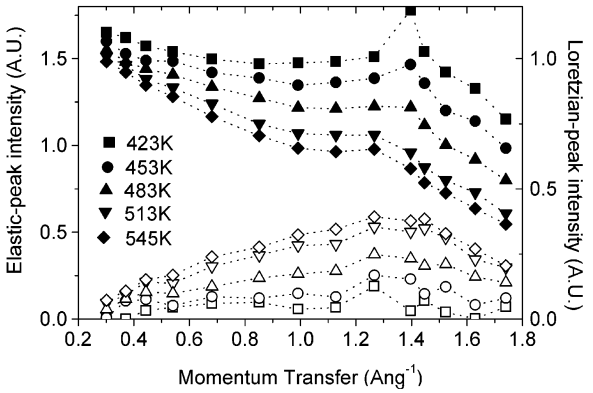


**Figure 9.** Comparison of the temperature dependence (523−545 K) of the structure factor for the slow process (open symbols) with the elastic peak structure factor (solid symbols). The maximum for the slow process at all temperatures arises at the same value as that in the elastic structure factor close to the melting point.

process than a rotational diffusion. However, for a simple jump rotation on the diameter of the HBA unit, the elastic incoherent structure factor (EISF = [elastic intensity]/[elastic + quasi-elastic intensity]) would show a minimum at 1.5 Å$^{-1}$, which is in conflict with the experimental data. Further, below $T_m$ the intensity of this peak (relative to the elastic peak) is only ∼0.2, which is too small for rotational diffusion of the HBA units (70% of the sample) but would be consistent with local translational motion of chain segments that would also have the correct polarization. While much of the interchain correlation is maintained despite these local translations, for large-amplitude monomer rotations the correlations between atoms on neighboring chains necessarily reduce. This is broadly consistent with discussion of $S(Q)$ at $\omega = 0$ given above.

**Phase from 383 to 553 K.** At 10 K above $T_g$ we were still able to fit a single Bergman function, but the values of all three parameters are significantly different from those below $T_g$. At higher temperatures a second function was required to adequately fit the data, and an additional simple Lorentzian was found to give adequate agreement with the experimental data. The temperature dependence of the Bergman function is more marked above $T_g$, the average relaxation time decreasing and the intensity increasing with temperature. $\beta$ also changes from a nearly constant value of 0.73 below $T_g$ to a constant 0.65 above the transition.

Inspection of Figure 8 shows the intensity of the Lorentzian function above $T_g$ to be linear with an intercept on the temperature axis that is close to $T_g$. This confirms that the peak is too narrow to resolve in the current experiments at 393 K and below. Figure 9 compares the $Q$ variation of the elastic peak intensity with that of the Lorentzian component at a number of temperatures above $T_g$. For the latter, the maximum intensity is at $Q = 1.3$ Å$^{-1}$ for all temperatures, while it can be seen from the elastic peak variation that the Bragg peak arising from the interchain distance broadens and shifts from 1.4 to 1.3 Å$^{-1}$ over the temperature range 423−545 K. This suggests that the length scale of the dynamics underlying the Lorentzian function in this phase is the same as the interchain spacing in the crystalline melt and that the increased amplitude of this motion may be the driving force for the transitions at 383 and 553 K. Further, although the global fitting procedure constrained the Lorentzian peak width to be constant with $Q$, use of an adjustable parameter for the width (for spectra at 545 K) reveals a measurable increase in the width above $Q \sim 1.5$ Å$^{-1}$, although the errors are significant. This observation also supports the idea that motion the length scale proposed above is the origin of the narrow Lorentzian quasi-elastic broadening.

The intensity loss of the elastic peak with increasing $Q$ in Figure 9 is mostly due to the broad quasi-elastic scattering. It is particularly noticeable at higher temperatures that, apart from the broad peak at around 1.3 Å$^{-1}$, this intensity loss is almost linear with $Q$. This is a simple manifestation of the linear increase in intensity of the broad quasi-elastic with increasing $Q$, and it would be interesting to extend a purely elastic measurement to much higher $Q$ values in order to order to obtain more information on the spatial development of the underlying dynamics.

The picture that emerges is of a dispersed translational motion below $T_g$ that becomes slightly more hindered on increasing temperature. Above $T_g$ we see a new slower motion arise on a length scale that is modulating the interchain spacing, around an average compatible with this spacing in the high-temperature nematic phase. This motion is considerably slower than the average relaxation of the Bergman function and does not show a measurable sign of dispersion. On the basis of the length scale, it seems likely that this slow dynamics is the so-called "crankshaft" motion of neighboring segments of the chain. Given the comparatively low torsional barrier of the bond-type marked "1" in Figure 1 (12.5 kJ mol$^{-1}$),[7] these would be the most important coordinates for this motion. With increasing amplitude this libration places the aromatic units in environments where the translational potential increases, leading to slower relaxation with increased dispersion ($\beta$).

This picture would suggest that the crankshaft dynamics to also exist below $T_g$, but with an amplitude and relaxation rate that are too small to measure in the current experiment.

## Conclusions

The evidence for dispersion in the fast process is clear, and this is not surprising. However, it is much more difficult to identify the relaxation processes themselves, and in the current work we have used overall intensity, diffuse scattering, structure factors, and $Q$ dependence of peak widths to obtain a consistent interpretation.

There are many aspects of disordered systems that can give rise to a distribution of relaxation processes, from simple static disorder through to relaxation processes that occur in an evolving environment, and in the current study we can make some comment on this. The temperature dependence of the diffuse elastic scattering allows us to establish the relative importance of slow dynamics disorder and to correlate this with the quasi-elastic signals. As a result, we propose that the slow librational/rotational process in HBA/HNA, which is observed here for the first time, causes the distribution of environments for the fast process. Because there is almost 2 orders of magnitude difference in the relaxation rates of the two processes, we can regard the dispersion as arising from an essentially static distribution. This distribution is thermally activated and is unusual because it hardens the distribution of barriers with increasing temperature, leading to the observed narrowing of the quasi-elastic signal with increasing temperature. The spectral intensity of the faster process increases linearly with $Q$ up to at least 1.8 $Å^{-1}$, and it would be interesting to collect good quality data up to much higher $Q$.

## References and Notes

(1) Lukacs, S. J.; Cohen, S. M.; Long, F. H. *J. Phys. Chem. B* **1999**, *103*, 6648.
(2) Lukacs, S. J. *J. Phys. Chem. B* **2001**, *105*, 3372.
(3) Koizumi, S. J. *Chem. Phys.* **1997**, *107*, 603.
(4) Koizumi, S. *Physica B* **1998**, *241*, 973.
(5) Koizumi, S.; Inami, T. *Macromolecules* **1999**, *32*, 5613.
(6) Donald, A. M.; Windle, H. H. *Liquid Crystalline Polymers;* Cambridge University Press: Cambridge 1992.
(7) Bharadwaj, R. K.; Boyd, H. H. *Macromolecules* **1998**, *31*, 7682.
(8) Ruiten, J. v.; Meier, R. J.; Hahn, C.; Mosell, T.; Sariban, A.; Brickmann, J. *Macromolecules* **1993**, *26*, 1556.
(9) Dingemans, T. J.; Weiser, E. S.; StClair, T. L. US Patent Application, 2001, 09/757,398.
(10) Bergman, R. J. *Appl. Phys.* **2000**, *88*, 1356.
(11) Hofmann, D.; Schneider, A. I.; Blackwell, J. *Polymer* **1994**, *35*, 5603.

MA0486849